RSC Advances

PAPER

View Article Online
View Journal | View Issue



Cite this: *RSC Adv.*, 2025, **15**, 31830

# Orthogonal design-driven *in situ* encapsulation of hyaluronic acid-poly (lactic acid) composite hydrogels: mechanically tunable dermal fillers with enhanced enzymatic resistance

Jiahong Guo, [ab] Hang Li[c] and Feifei Wang*[ad]

Injectable hyaluronic acid (HA) – based hydrogels face limitations in clinical longevity due to enzymatic degradation and insufficient mechanical stability. To address these challenges, this study developed a novel *in situ* encapsulation strategy for fabricating crosslinked HA-poly(L-lactic acid) (PLLA) composite hydrogels (CHPs), optimized *via* an $L_{16}$ ($4^3$) orthogonal experimental design. Three critical parameters – PLLA loading (0–10% w/v), 1,4-butanediol diglycidyl ether (BDDE) concentration (0.5–2% w/v), and crosslinking time (8–72 h) – were systematically evaluated to balance viscoelasticity, injectability, and biocompatibility. The optimized formulation (3% PLLA, 1.0% BDDE, 48 h crosslinking) achieved a storage modulus ($G'$) of 790 Pa, demonstrating 2.3-fold enhancement over conventional post-mixing dispersion (PMD) hydrogels. Mechanistic studies revealed hydrogen bonding between HA hydroxyl/carboxyl groups and PLLA carbonyl moieties, which compensated for steric hindrance-induced crosslinking inefficiency at moderate PLLA loading. CHPs fabricated *via in situ* encapsulation exhibited superior enzymatic resistance, with degradation rates lower than PMD counterparts. This work establishes *in situ* encapsulation as a scalable methodology for engineering HA-PLLA composites, offering a transformative platform in designing durable, biocompatible dermal fillers with tunable mechanical and degradation profiles.

Received 16th June 2025
Accepted 27th August 2025

DOI: 10.1039/d5ra04259c

rsc.li/rsc-advances



## Introduction

Injectable hydrogels based on hyaluronic acid (HA) have garnered significant attention in regenerative medicine and aesthetic dermatology due to their inherent biocompatibility, biodegradability, hydrophilicity, and viscoelastic adaptability.[1–3] As a naturally occurring glycosaminoglycan, HA plays a pivotal role in maintaining tissue hydration and structural integrity, making it an ideal candidate for dermal fillers.[4–6] However, the rapid enzymatic degradation and insufficient mechanical stability of conventional HA hydrogels often limit their clinical longevity, necessitating innovative strategies to enhance their performance.[7]

Recent advancements in composite hydrogels have focused on incorporating reinforcing agents such as PLLA microspheres, lithium calcium silicate ($Li_2Ca_4Si_4O_{13}$), hydroxyapatite, and polycaprolactone (PCL) to enhance mechanical and bioinductive properties.[8–11] These tissue-responsive fillers not only provide structural reinforcement but also stimulate collagen synthesis through cellular activation triggered by gradual hydrogel degradation.[12,13] For instance, SculptraTM, an FDA-approved dermal filler comprising carboxymethylcellulose sodium (CMC-Na) and PLA, demonstrates clinical efficacy but suffers from particle agglomeration during injection, leading to uneven distribution and compromised aesthetic outcomes.[14] To address this, high-viscosity carriers or covalently crosslinked hydrogel matrices have emerged as promising alternatives stabilize particulate dispersions. Zhao *et al.* developed a PLA-embedded HA composite hydrogel; however, the use of submicro-sized PLA powders inadvertently increased risks of vascular occlusion and tissue necrosis due to unintended intravascular migration.[8,15]

A critical challenge lies in optimizing fabrication parameters – including crosslinker concentration, polymer loading, and reaction kinetics – to balance mechanical resilience, injectability, and biocompatibility. Traditional full-factorial experimental designs, though thorough, are resource – intensive and impractical for multifactorial system. Orthogonal experimental design (OED) offers a statistically robust alternative, enabling efficient exploration of parameter interactions with minimized experimental burden.[16–18]

[a]*Yunnan Botanee Bio-technology Group Co., Ltd, Yunnan 650106, China. E-mail: wangfeifei@botanee.com*
[b]*Shanghai Jiyan Bio-pharmaceutical Co., Ltd, Shanghai 201702, China*
[c]*Shanghai Botanee Health Technology Co., Ltd, Shanghai 201706, China*
[d]*Yunnan Characteristic Plant Extraction Laboratory Co., Ltd, Yunnan 650106, China*

This study introduces a new *in situ* encapsulation methodology for fabricating covalently crosslinked HA-PLLA composite hydrogels (CHPs), addressing critical limitations of conventional post-mixing dispersion approaches. Unlike existing methods that physically blend PLLA into pre-crosslinked HA networks, the *in situ* strategy integrates PLLA microspheres during precursor gel formation, fostering molecular-level interactions prior to covalent crosslinking. This sequential fabrication not only enhances interfacial bonding but also mitigates steric hindrance effects that compromise crosslinking efficiency.

Through an $L_{16}$ ($4^3$) orthogonal experimental design, three pivotal parameters – PLLA loading, BDDE concentration, and crosslinking duration – were systematically optimized. The resultant hydrogels were rigorously characterized for viscoelasticity, degradation kinetics, and injectability, with comparative analysis against post-mixing dispersion counterparts. We further elucidated the mechanistic role of hydrogen bonding between HA's hydroxyl/carboxyl groups and PLLA's carbonyl moieties, revealing a concentration-dependent reinforcement effect. By bridging material innovation with methodological optimization, this work advances the rational design of injection hydrogels, offering a scalable platform for next-generation dermal fillers that harmonize clinical efficacy with regulatory safety standards.

# Experimental

## Materials

Sodium hyaluronate (HA, Mw = 1 800 000 Da) was purchased from Shandong TopScience Biotech Co., Ltd (Shandong, China). Poly(L-lactic) (PLLA) microspheres were obtained from Sichuan Yizheng Medical Technology Co., Ltd (Sichuan, China). 1,4-Butanediol diglycidyl ether (BDDE), hyaluronidase, sodium hydroxide, hydrochloric acid (HCl), glucuronic acid, carbazole, sodium tetraborate, ethanol, and sulfuric acid were purchased from Sigma-Aldrich Chemical Co., Ltd (Shanghai, China). Potassium hydroxide, acetophenone, formic acid, and nicotinamide were sourced by Sinopharm Chemical Reagent Co., Ltd (Shanghai, China). Sodium chloride (NaCl) was supplied from Jiangsu Province Qinfen Pharmaceutical Co., Ltd (Jiangsu, China). Sodium hydrogen phosphate and sodium dihydrogen phosphate were acquired from Jiudian Hongyang Pharmaceutical Co., Ltd (Hunan, China).

## Fabrication of CHPs hydrogels *via in situ* encapsulation

To prepare the composite hydrogels, HA powders (12%, w/v) was first completely dissolved in 1% sodium hydroxide (NaOH) solution under continuous stirring to form a homogeneous HA precursor gel. Subsequently, varying concentrations of PLLA microspheres (0–10%, w/v) were uniformly dispersed into the HA precursor gel. After thorough mixing, the crosslinking agent BDDE was added, and the reaction was allowed to proceed at 25 °C for a predetermined duration. Upon completion of crosslinking, the resulting composite hydrogel was sectioned into fragments (<1 $cm^3$) and neutralized with 1mol per L HCl. To facilitate swelling, phosphate-buffered saline (PBS, 2–4 times of hydrogel volume) was added. After full absorption of PBS, the hydrated hydrogels were mechanically fragmented using a pulverizer. The crushed hydrogels were dialyzed against PBS (cellulose membrane, MWCO 14 000 Da) for 5 days to eliminate any remaining BDDE. The experimental parameters, including PLLA loading, BDDE concentration, and crosslinking time, are summarized in Table 1. The resultant hydrogels were designated as formulation number in orthogonal experiment and CHP-*n*% ($n$ = 0–10%) based on PLLA content.

Table 1 Orthogonal experimental combination and result of rheology

| | Fabrication parameters | | | Results | | |
|---|---|---|---|---|---|---|
| Formulation number | PLLA ($f$, %) | BDDE ($c$, %) | Time ($t$, h) | Gel | $G'$ | $G''$ |
| 1 | 0 | 0.5 | 8 | × | | |
| 2 | 0 | 1 | 24 | √ | 346 | 40 |
| 3 | 0 | 1.5 | 48 | √ | 922 | 131 |
| 4 | 0 | 2 | 72 | √ | 1428 | 422 |
| 5 | 3 | 0.5 | 24 | √ | 189 | 53 |
| 6 | 3 | 1 | 48 | √ | 790 | 160 |
| 7 | 3 | 1.5 | 72 | √ | 1509 | 274 |
| 8 | 3 | 2 | 8 | √ | 173 | 55 |
| 9 | 6 | 0.5 | 48 | √ | 71 | 48 |
| 10 | 6 | 1 | 72 | √ | 145 | 59 |
| 11 | 6 | 1.5 | 8 | √ | 185 | 66 |
| 12 | 6 | 2 | 24 | √ | 831 | 123 |
| 13 | 10 | 0.5 | 72 | × | | |
| 14 | 10 | 1 | 8 | √ | 119 | 66 |
| 15 | 10 | 1.5 | 24 | √ | 141 | 56 |
| 16 | 10 | 2 | 48 | √ | 292 | 157 |

## Fabrication of CHPs hydrogels *via* post-mixing dispersion

The key distinction between the post-mixing dispersion method and the *in situ* encapsulation approach lies in the sequential addition PLLA microspheres. Briefly, HA powders (12%, w/v) was dissolved in 1% NaOH at ambient temperature to form a homogeneous solution. BDDE was then incorporated, and crosslinking proceeded at 25 °C. Following crosslinking, the hydrogel was processed identically to *in situ* polymerization (fragmentation, neutralization, swelling, and pulverization). After dialysis, PLLA microspheres were homogenously blended into the HA matrix under stirring. The final product was labeled as CHP-PMD.

## Characterization of CHPs hydrogels

The chemical structures of PLLA powders and lyophilized CHPs hydrogels were characterized by attenuated total reflectance Fourier-transform infrared spectroscopy (ATR-FTIR, iS10, Thermo Nicole) over the range of 4000 to 400 $cm^{-1}$ at ambient temperature. The storage modulus ($G'$), viscous modulus ($G''$) were determined using a rheometer (HR-10, Waters TM) with a 20-mm steel plate geometry. Frequency sweep tests were conducted under oscillatory shear (1.0% strain, 0.1–100 Hz,

1 mm gap) at temperature of 37 °C. Morphological analysis was performed *via* field-emission scanning electron microscopy (FE-SEM, Hitachi, TM 4000) after sputter-coating with gold for a better conductivity. Optical microscopy (Leica, DM2700M) was employed to assess PLLA microspheres distribution. Injectability was quantified using a texture analyzer (AMETEK Brookfield, CTX) with controlled extrusion parameters (27 G needle, 0.5 mm per s displacement rate). pH and osmolality measurements were conducted using calibrated instruments (Metter Toledo, S210 pH meter; Löser, OM819. C osmometer), with NaCl/$H_2O$ solutions serving as calibration standards.

### Quantification of HA concentration

HA concentration was determined through carbazole–glucuronic acid chromogenic reaction. CHPs hydrogel samples ($m_1$, density 1.01 g mL$^{-1}$) were hydrolyzed in 0.5 mol per L $H_2SO_4$ at 95 ± 5 °C until complete dissolution, followed by neutralization with 1 mol per L NaOH and volumetric dilution to $m_2$ (density 1.00 g mL$^{-1}$). Concurrently, glucuronic acid standard solutions (0–50 μg mL$^{-1}$) were prepared. Both samples and standards underwent identical derivation: ice-bath incubation with 5 mL $Na_2B_4O_7$–$H_2SO_4$ (0.025 mol L$^{-1}$), boiling for 15 min, addition of 0.2 mL carbazole/ethanol, and secondary boiling for chromophore development. After cooling to ambient temperature, absorbance at 530 nm was measured using a microplate reader (Molecular Devices, i3x). The HA concentration $\rho$ (mg mL$^{-1}$) was calculated *via* the following eqn (1):

$$\rho = 2.0675 \times \rho_{\text{sam}} \times \frac{m_2 \times \rho_1}{m_1 \times \rho_2} \quad (1)$$

where $\rho_{\text{sam}}$ (μg mL$^{-1}$) denotes glucuronic acid concentration, $m_1$ (μg) and $m_2$ (mg) represent the initial CHPs and diluted masses, with $\rho_1 = 1.01$ g mL$^{-1}$ and $\rho_2 = 1.00$ g mL$^{-1}$.

### Residual BDDE analysis

The test of residual BDDE content can be examined by detecting the fluorescence intensity of substances produced by BDDE and nicotinamide where the excitation and emission wavelengths are located at 370 and 430 nm, respectively. Hydrogel samples were enzymatically digested with hyaluronidase (2000 U mL$^{-1}$, 37 °C, 24 h, 70 rpm) and subsequently derivatized by sequential addition of 125 mM nicotinamide (37 °C, 2 h), alkaline cleavage with 1 mol per L KOH/15% acetophenone (ice bath, 10 min), and formic acid activation (60 °C, 5 min). Calibration standards (0.25–8 μg per mL BDDE) underwent identical treatment. Fluorescence intensity was measured using ELIASA (Molecular Devices, i3x), with interpolation from the standard curve.

### *In vitro* enzymatic degradation

The enzymatic degradation of crosslinked HA hydrogels was monitored through hyaluronidase-induced structural cleavage, which generates unsaturated disaccharides and reduces HA content. To be brief, CHPs hydrogels ($m_1$) were subjected to hyaluronidase digestion (30 U mL$^{-1}$ in 5 mL PBS, 37 °C) over time intervals (15 min–7 h). Post-digestion processing involved multiple PBS rinses to collect degradation byproducts, followed by transfer to pre-weight tubes ($m_2$) and homogenization. A 500 μL aliquot was centrifuged (4000 rpm, 10 min) through 10 kDa ultrafiltration membranes to isolate degradation fragments. The filtrate was diluted appropriately and analyzed for glucuronic acid content using the carbazole assay described in quantification of HA concentration, with parallel preparation of glucuronic acid standard (0–50 μg mL$^{-1}$). The degradation percentage ($D_e$) was calculated according to the following eqn (2).

$$\text{De} = \frac{2.0675 \times G \times \dfrac{m_2 \times \rho_1 \times n}{m_1 \times \rho_2}}{H \times 1000} \times 100\% \quad (2)$$

where De (%) is the degradation rate of CHPs. $m_1$ (μg) and $m_2$ (mg) represent the initial CHPs and diluted masses, with $\rho_1 = 1.01$ g mL$^{-1}$ and $\rho_2 = 1.00$ g mL$^{-1}$. $G$ (μg mL$^{-1}$) represent the glucuronic acid concentration. $H$ (mg mL$^{-1}$) represents the initial HA concentration of CHPs, and $n$ is the diluted factor.

### Statistical analyses

Data are presented as mean ± standard deviation from at least three independent experiments. The statistical significance between two groups was determined by Student's *t*-test or one-way ANOVA with Bonferroni post hoc correction. A difference was regarded as significant if $p < 0.05$ in a test, unless otherwise indicated.

## Results and discussion

Orthogonal experimental design provides an efficient statistical approach for investigating multifactorial systems with potential interactions.[19] This methodology becomes particularly advantageous when examining three or more variables, as conventional full-factorial investigations (requiring 64 combinations for $4^3$ variables) become prohibitively resource-intensive.[18] In our system, three critical fabrication parameters were optimized: PLLA feed concentration ($f$), BDDE concentration ($c$), and crosslinking time ($t$), each examined at four levels. Through implementation of an $L_{16}$ ($4^3$) orthogonal experimental design, we systematically reduced experimental permutations from 64 to 16 while maintaining statistical validity (Table 1). This strategic reduction enabled comprehensive evaluation of parameter interactions with minimized experimental expenditure.[20]

Rheological characterization revealed significant combinatorial effects of $f$, $c$, and $t$ on hydrogel viscoelasticity (Table 1). Notably, 87.5% of formulations (14/16) achieved successful crosslinking, evidenced by storage modulus ($G'$) exceeding loss modulus ($G''$). The two-exceptions-formulations 1 and 13 – demonstrated characteristic uncrosslinked behavior. Formulation 1 (pure HA without PLLA) likely failed due to subcritical BDDE concentration (0.5% w/v) combined with insufficient crosslinking duration (8 h). Conversely, formulation 13's failure may stem from excessive PLLA loading (10% w/w) and little BDDE concentration (0.5% w/v) compromising network formation despite enough crosslinking time (72 h).

Frequency-dependent rheological analysis of successful formulations (Fig. 1A and B) demonstrated broad viscoelastic

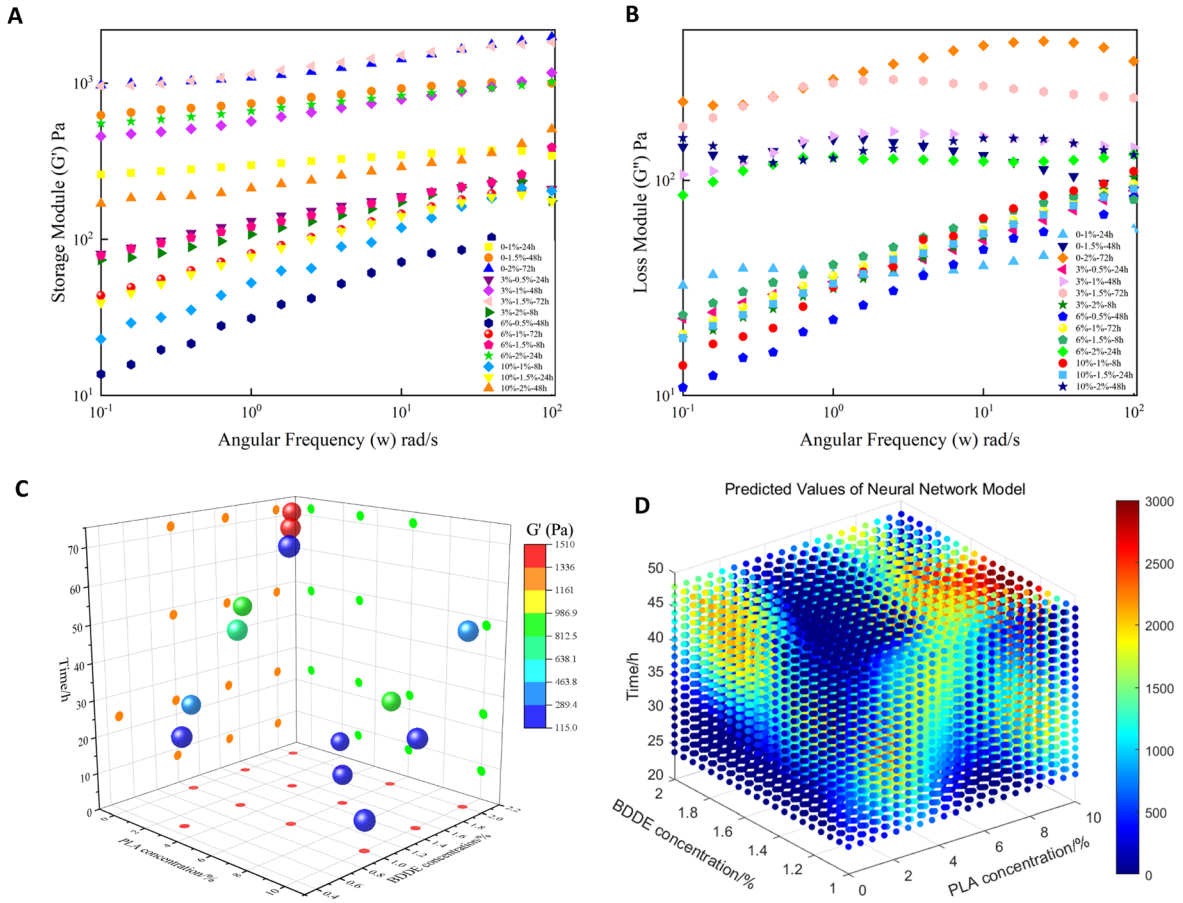


Fig. 1 Rheological characterization and predictive model validation of orthogonal experimental design outcomes. Storage module ($G'$) profiles (A) and loss module ($G''$) profiles (B) across formulation variants. The viscoelastic characterization (C) and predictive model validation (D) of orthogonal experimental results. The chromatic gradation transitioning from blue to red corresponds to a progressive enhancement in elastic modulus magnitude, delineating the quantitative relationship between formulation parameters and mechanical response characteristics.

tunability, with $G'$ ranging from 71 Pa (formulation 9) to 1509 Pa (formulation 7). Three-dimensional parameter-response surface modeling (Fig. 1C) revealed distinct correlations: chromatic gradation transitioning from blue to red illustrated dose-dependent enhancement with increasing $c$ and $t$, while $f$ exhibited non-monotonic influence.

A predictive model validation was developed using MATLAB R2021a, achieving high prediction accuracy for $G'$ within the experimental parameter space, as shown in Fig. 1D. This computational framework enables: (1) targeted hydrogel design meeting clinical mechanical specifications (100–2000 Pa, per commercial dermal filler benchmarks), (2) identification of manufacturing-efficient parameter sets, and (3) reduction of post-processing burdens. For instance, while elevated BDDE concentrations enhance crosslinking efficiency, they necessitate prolonged purification to maintain residual BDDE < 2 ppm.[14]

Through multi-criteria optimization balancing mechanical performance, process efficiency, and potential biocompatibility, formulation 6 emerged as optimal: 3% PLLA (w/w), 1.0% BDDE (w/v), and 48 h crosslinking. This combination achieved $G'$ = 790 Pa with low BDDE residual within standard purification protocols, demonstrating the methodology's translational potential for injectable dermal filler.

To elucidate the concentration-dependent effects of PLLA microspheres on hydrogel mechanical property, we conducted controlled rheological studies with systematic PLLA variations (0–10% w/v) under fixed crosslinking conditions (1.0% BDDE, 48 h). As evidenced in Fig. 2, the storage modulus ($G'$) demonstrated a biphasic response to PLLA loading: formations containing 2–8% PLLA exhibited 35–120% enhancement in $G'$ compared to PLLA controls (CHP-0%), while CHP-10% regained baseline stiffness ($p < 0.05$). This mechanical reinforcement aligns with PLLA's inherent material property – high Young's modulus (3.0–5.3 GPa) and surface hydrophobicity (contact angle >130°) – which collectively enhance composite rigidity through particulate reinforcement mechanisms.[21–23] Notably, the observed strengthening phenomenon showed methodological universality, being reproducible in both *in situ* encapsulation and conventional pre-mixing approaches. Here, we only discuss the viscoelasticity of the CHPs fabricated by *in situ* encapsulation method. With the increase of PLLA feed loading, the storage modulus exhibited increase first and then decrease. When PLLA loading lower than 4%, FTIR-identified hydrogen

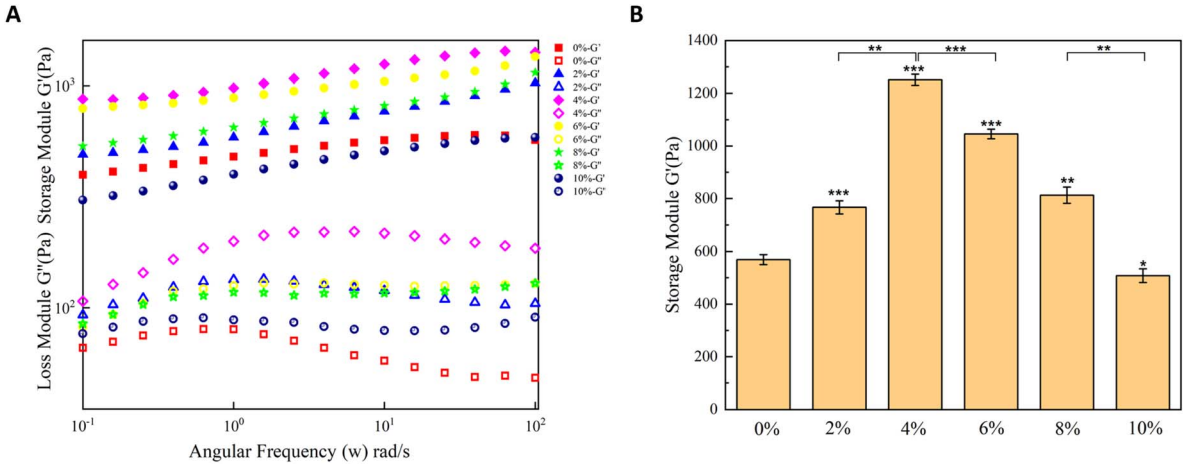


Fig. 2 Rheological behavior and viscoelastic quantification of CHPs modulated by PLLA feed concentration (0–10% w/v). (A) The frequency-dependent viscoelastic profiles. (B) Storage modules ($G'$) magnitudes across concentration gradients. Error bars denote triplicate measurements ($n = 3$). Statistical annotations (*$p < 0.05$, **$p < 0.01$, ***$p < 0.001$).

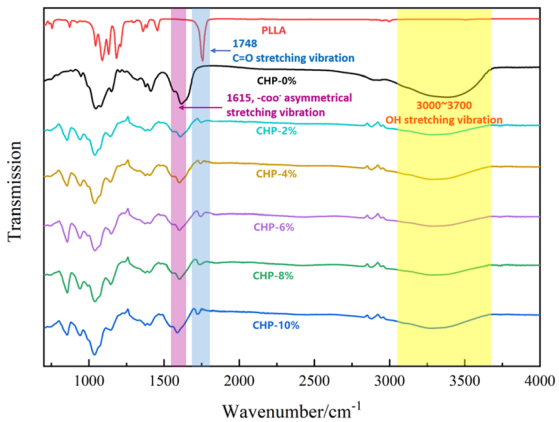


Fig. 3 The FTIR spectra of PLLA and CHPs modulated by PLLA feed concentration (0–10% w/v).

bonding between PLLA carbonyl group (C=O) and HA proton donors (–OH/–COOH) (Fig. 3). When PLLA loading larger than 4%, the steric hindrance effects decreased the contact possibility between HA and BDDE, significantly reduced the crosslinking efficiency between HA and BDDE. This competition explains the optimized performance at 4% PLLA, where hydrogen bond reinforcement outweighs crosslinking inhibition effects. Notably, the optimal formulation (4% PLLA) achieved clinically compatible viscoelasticity ($G' = 1251$ Pa), while maintaining structural stability ($\tan\delta < 0.2$ across 0.1–10 Hz). This finding almost aligns with our orthogonal experimental result, confirming the robustness of *in situ* encapsulation methodology.

The chemical structures of PLLA and CHPs were characterized by Fourier Transform Infrared (FTIR) spectroscopy as illustrated in Fig. 3. All CHPs samples exhibited characteristic polysaccharide –OH stretching vibrations of hyaluronic acid (HA) within the 3000–3700 $cm^{-1}$ region.[24] Notably, the CHP-0% sample demonstrated significantly higher peak intensity in this region compared to other groups, which can be attributed to its composition as a pure crosslinked HA hydrogel devoid of PLLA microspheres. In contrast, the FTIR spectrum of pristine PLLA displayed distinct features, particularly the absence of absorption peaks in the 3000–3700 $cm^{-1}$ range characteristic of HA-based materials. Critical spectral signatures were observed at 1615 $cm^{-1}$ and 1748 $cm^{-1}$, corresponding to the asymmetrical stretching vibrations of HA carboxyl groups (–COOH) and the carbonyl (C=O) stretching vibration of PLLA, respectively. These diagnostic peaks co-appeared in all PLLA-containing CHP groups, while their absence in control spectra provided compelling evidence: Specifically, the 1748 $cm^{-1}$ peak was absent in CHP-0% and the 1615 $cm^{-1}$ peak did not appear in pure PLLA spectra. This reciprocal absence confirms the successful incorporation of PLLA microspheres within the HA hydrogel matrix. Notably, both characteristic peaks exhibited measurable spectral shifts (redshift) accompanied by peak broadening, suggesting the formation of hydrogen-bonding interactions between the hydroxyl and carboxyl groups of HA and PLLA carbonyl moieties. This further confirmed the possibility that a small amount PLLA loading can enhance the storage module of CHPs (Fig. 2).[8,25] Furthermore, the magnitude of these spectral modifications showed a concentration-dependent relationship, with more pronounced effects observed in formulations containing higher PLLA loading percentages. This phenomenon implies that increased PLLA content enhances interactions between the hydrogel matrix and embedded microspheres.

The microstructural characteristic of CHPs hydrogels was systematically investigated through field-emission scanning electron microscopy (FE-SEM) analysis, as illustrated in Fig. 4 (200× magnification) and Fig. 1S (500× magnification). All CHPs hydrogels maintained a three-dimensional interconnected porous architecture following PLLA incorporation, suggesting preservation of the hydrogel's inherent network structure post-loading. The hierarchical porous architecture demonstrates dual biological significance: (1) providing

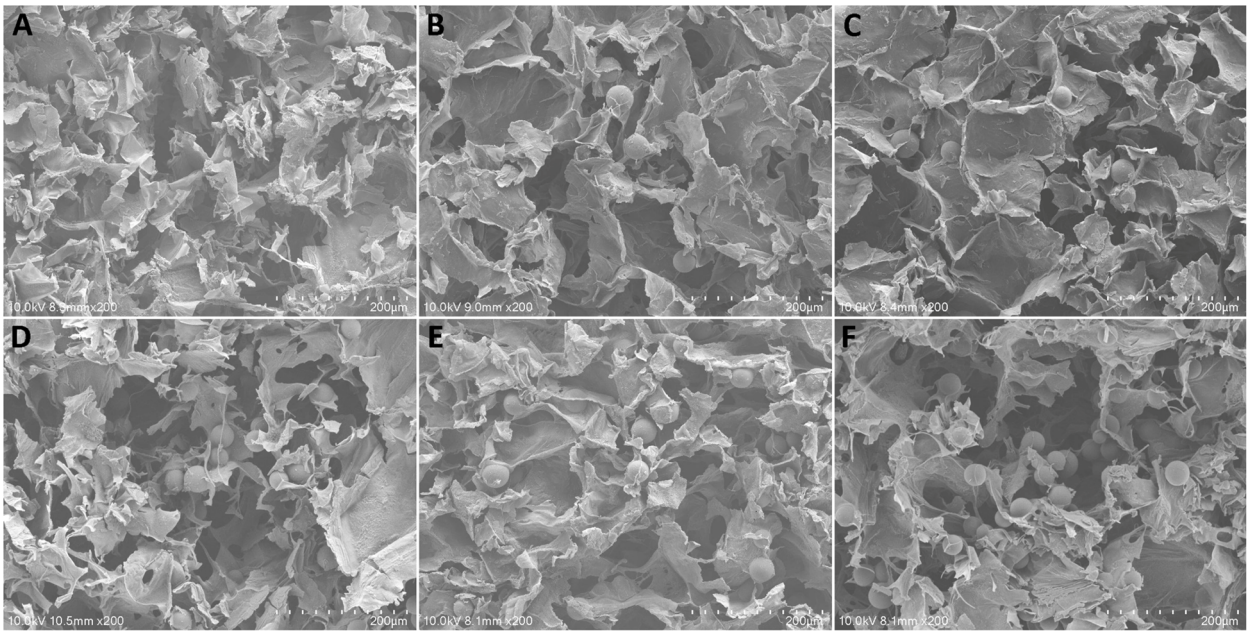


Fig. 4 Morphological evolution of CHPs as a function of PLLA feed loading. (A–F) Loading-dependent topological transition (0%, 2%, 4%, 6%, 8%, 10% w/v) captured at 200× magnification.

structural guidance for cellular infiltration, and (2) serving as a bioactive scaffold that enhances fibroblast proliferation while activating critical pathways associated with extracellular matrix remodeling.[26,27]

Notably, qualitative analysis demonstrated a positive correlation between PLLA feed loading and pore dimension enlargement, contrasting with the denser morphology observed in CHP-0%. This structure evolution could be attributed to reduced crosslinking density resulting from steric hindrance effects induced by PLLA incorporation, which consequently generates more loosely packed polymeric networks. Remarkably, the spherical geometry of PLLA microspheres remained structurally intact without observable damage during the encapsulation process within non-crosslinked HA matrices. From spatial distribution analysis, predominant embedding of PLLA microspheres within the hydrogel's porous cavities, with limited instances of surface adhesion on the lamellar structures of lyophilized CHPs.

High-resolution imaging (Fig. 1S) unveiled distinct surface modification phenomena. Compared to pristine PLLA microspheres exhibiting characteristic smooth surfaces with the size ranging from 25–30 μm, the majority of incorporated microspheres displayed conformal coating composed of fibrous HA-crosslinked hydrogel network. Intriguingly, the thickness of these fibrous encapsulations exhibited an inverse relationship with PLLA loading concentration, likely governed by competitive molecular interactions and steric exclusion effects within the composite system.

A comparative evaluation was conducted between the novel *in situ* encapsulation methodology (ISE) and conventional post-mixing dispersion technique (PMD) for fabricating composite hydrogels. As illustrated in Fig. 5, *in situ* encapsulation approach involved sequential dispersion of PLLA microspheres within HA precursor gels followed by covalent crosslinking, thereby achieving three-dimensional network entrapment of particulate components. In contrast, the post-mixing dispersion method employed mechanical homogenization of PLLA microspheres into pre-crosslinked HA hydrogel matrices, representing typical physical blending strategy.

In the *in situ* encapsulation approach (ISE), the presence of uniformly dispersed PLLA microspheres within non-crosslinked HA precursor gels physically impedes the spatial proximity and reactivity potential between hydroxyl groups of HA and epoxide groups of BDDE (Fig. 2S), resulting in less dense crosslinked networks compared to pre-crosslinked HA hydrogel matrices fabricated through post-mixing dispersion. Notably, hydrogen-bonding interactions between the hydroxyl and carboxyl groups of HA and PLLA carbonyl moieties compensate for this structural deficiency, with suitable concentration demonstrating significantly enhanced interfacial strength over PMD systems. The enhancement arises from intensified molecular interactions during precursor mixing, enabling the formation of HA-crosslinked hydrogel coating both on PLLA microsphere surfaces and within their surrounding matrix (Fig. 6A). In contrast, the post-mixing dispersion method preserves complete HA-BDDE crosslinking prior to PLLA incorporation, generating denser hydrogel networks. However, subsequent introduction of PLLA microspheres induces structural deformation through mechanical displacement of established crosslinks. Network entanglements and crosslinking reaction reduced available HA functional groups (hydrogel and carboxyl), consequently weakening PLLA-HA interfacial interactions. Microstructural evidence also

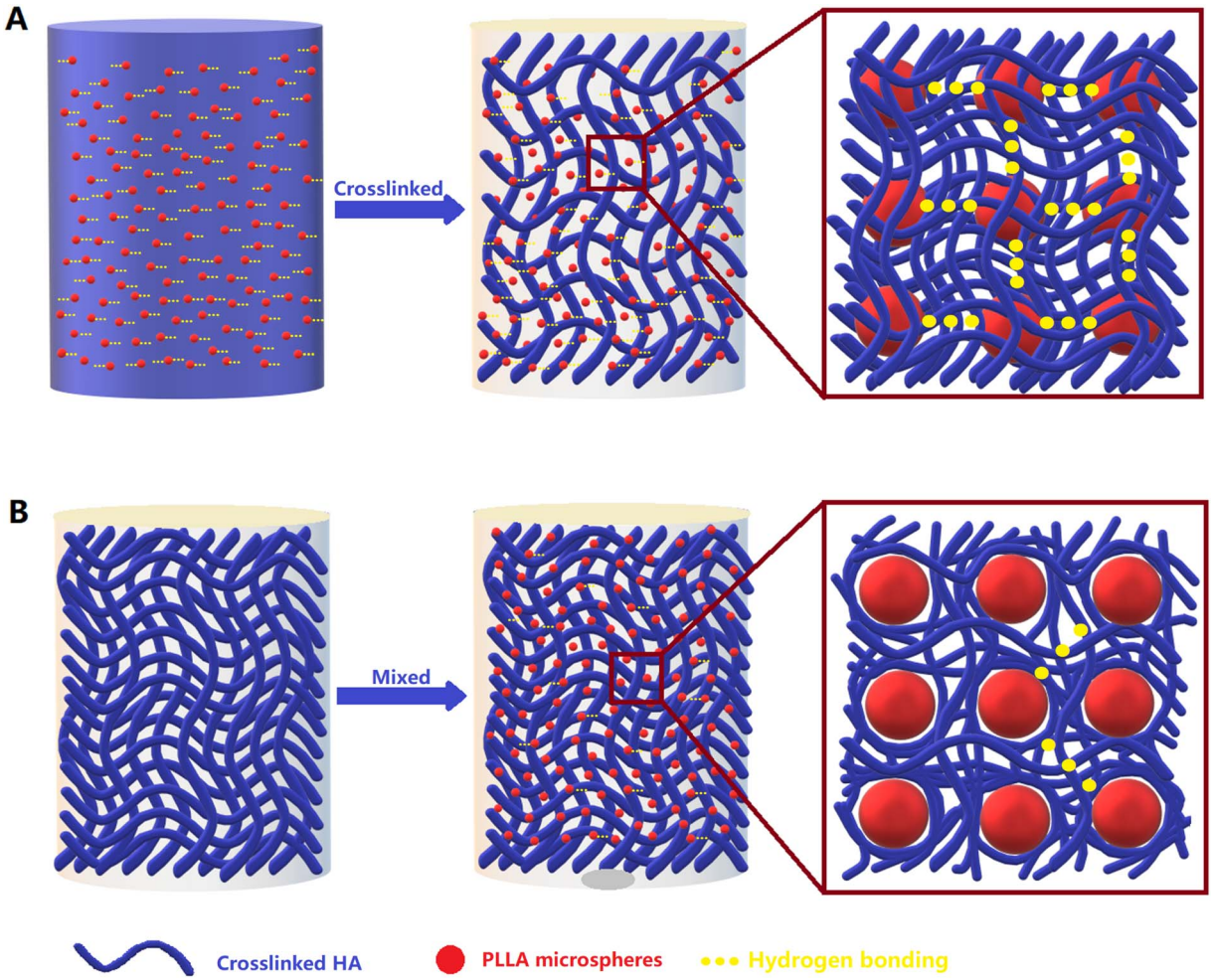


Fig. 5 Schematic illustration of two fabrication strategies for crosslinked HA hydrogels/PLLA microspheres composites (CHP). (A) *In situ* encapsulation: PLLA microspheres embedded within covalently crosslinked HA networks *via* sequential dispersion and crosslinking; (B) post-mixing dispersion: mechanical blending of PLLA microspheres into pre-crosslinked HA hydrogel matrices.

confirmed this mechanism, revealing smooth PLLA surfaces devoid of HA coatings in PMD systems (Fig. 6B).

Critical fabrication parameters were systematically optimized through orthogonal experiment design. For the *in situ* encapsulation protocol, optimal conditions were established as: 3 wt% PLLA loading, 1.0% w/v BDDE concentration, and 48 h crosslinking duration. In the post-mixing dispersion control group, equivalent BDDE concentration (1.0% w/v) and crosslinking time (48 h) were maintained, while PLLA content was adjusted to 0.55 wt% to match the final composite concentration in ISE. Morphological analysis (Fig. 6C and D) revealed comparable PLLA microsphere ratios and structures in both systems, with intact spherical morphology observed under optical microscope. This confirmed that neither pre-mixing nor post-mixing strategies compromised the structural integrity of PLLA microspheres.

The viscoelastic characteristics of CHPs fabricated *via in situ* encapsulation (ISE) and post-mixing dispersion (PMD) methodologies were comparatively presented in Fig. 7. Frequency sweep analysis revealed dominant elastic behavior in both systems, as evidenced by storage modulus ($G'$) values consistently exceeding loss modulus ($G''$) throughout the tested frequency range. Notably, ISE-processed CHPs exhibited a $G'$ of 790 Pa, representing a 2.3-fold enhancement over PMD counterparts (338 Pa). This indicated stiffness improvement substantiates the strategic advantage of incorporating PLLA microspheres into non-crosslinked HA precursor gels prior to network formation, as opposed to physical blending with pre-crosslinked HA hydrogel matrices. The observed mechanical superiority aligns with the interfacial enhancement mechanisms detailed in Fig. 5. Specifically, ISE method promotes molecular-level interactions between PLLA and HA before hydrogel crosslinking, whereas PMD approach only permits limited interactions with pre-crosslinked networks. This fundamental difference in fabrication sequence directly impacts the density of interfacial bonding sites, thereby dictating the ultimate mechanical performance.

Degradation resistance, a critical determinant of hydrogel longevity, was quantitatively assessed through *in vitro* enzymatic digestion under physiological conditions (pH 7.2, 30 U

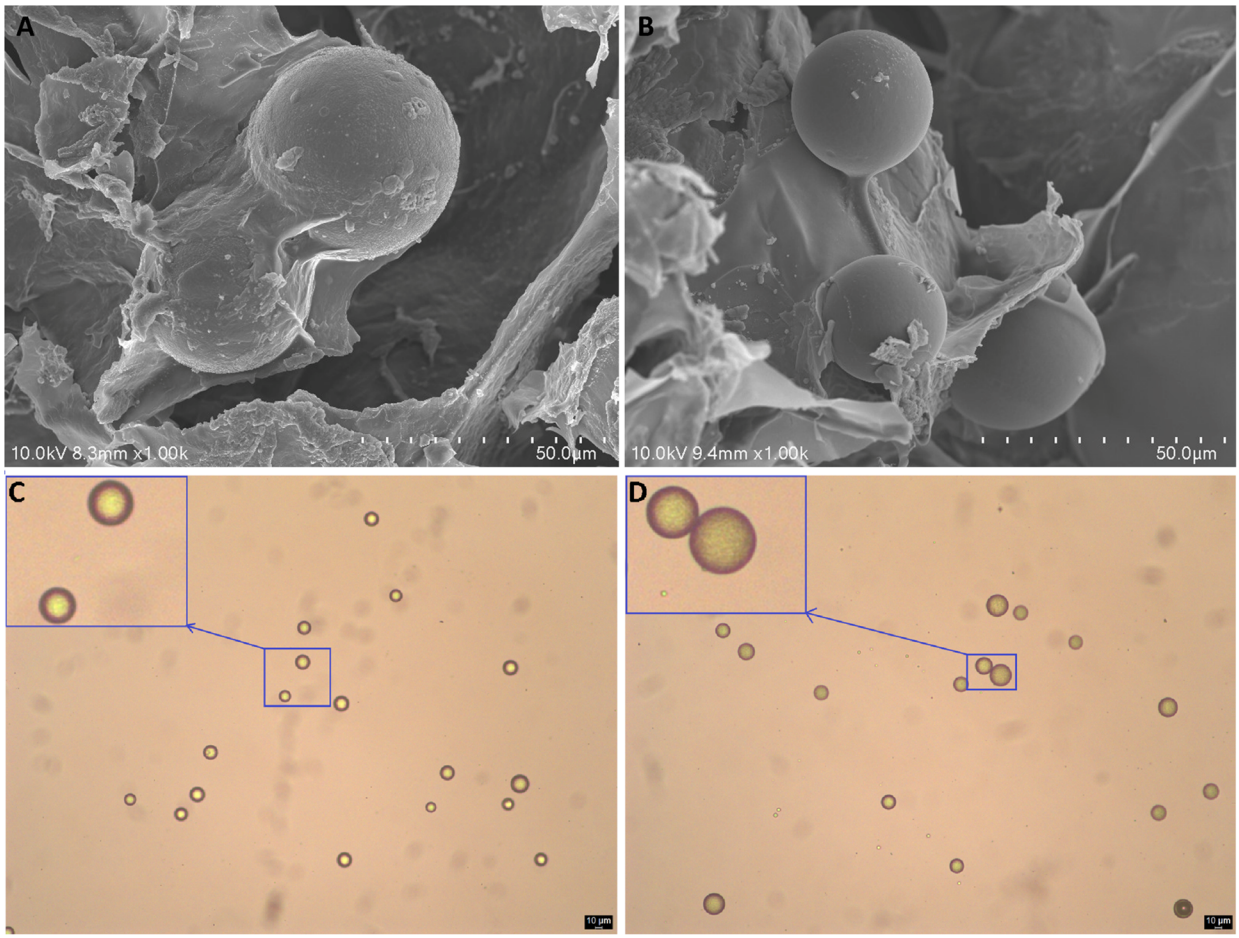


Fig. 6 The morphologies of the PLLA microspheres fabricated by (A and C) *in situ* encapsulation and (B and D) post-mixing dispersion. Images acquired using: (A and B) scanning electron microscopy (SEM); (C and D) optical microscopy.

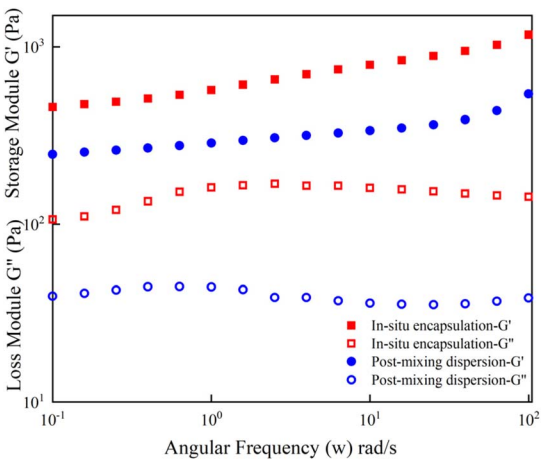


Fig. 7 The rheology behavior of the CHPs fabricated by *in situ* encapsulation (ISE) and post-mixing dispersion (PMD).

per mL hyaluronidase). The degradation kinetics were monitored *via* D-glucuronide quantification – a stoichiometric byproduct of HA hydrolysis exhibiting positive correlation with degradation rate. As demonstrated in Fig. 8A, CHPs fabricated by ISE displayed significantly attenuated degradation kinetics compared to CHP fabricated by PMD, confirming the enhanced durability of *in situ* encapsulation systems. This phenomenon is mechanistically attributed to: (1) superior structural resilience from higher elastic modulus (790 Pa *vs.* 338 Pa) resisting enzymatic penetration; (2) denser network topology physically restricting hyaluronidase accessibility.

Injection force constitutes an essential aspect in clinical therapeutics, directly impacting both procedural efficacy and patient safety. Excessive injection forces may cause compromise vascular integrity and induce patient discomfort, whereas controlled low-pressure administration is generally considered clinically safer by minimizing risks of vascular trauma and intravascular regurgitation.[24,28] Notably, injectability assessment through 27-gauge needles (Fig. 8B) revealed comparable extrusion forces between CHPs fabricated by ISE and PMD, despite ISE's marked storage modulus advantage. This apparent paradox may be attributed to two synergistic mechanisms: (1) structural homogeneity limitations: while ISE's uniformly distributed crosslinking points confer superior elastic deformation characteristics and consequently higher storage modulus, the absence of energy dissipation pathways (*e.g.*, network fracture or polymer chain slippage) ultimately limits

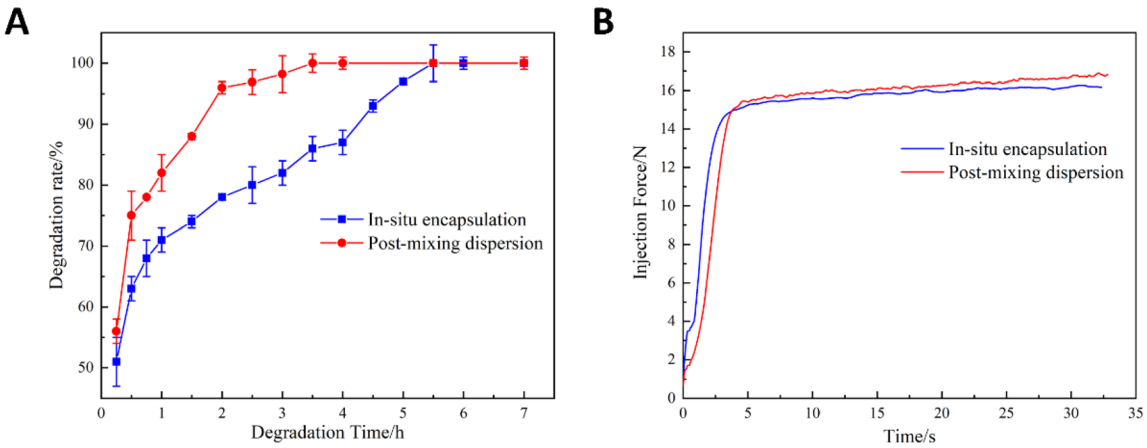


Fig. 8 The degradation behaviors (A) and injection force characterization (B) of the CHPs hydrogels fabricated by *in situ* encapsulation and post-mixing dispersion methods. Error bars denote triplicate measurements ($n = 3$).

force transmission during injection. (2) Dynamic bond reorganization: the reversible hydrogen – bonding interactions between PLLA microspheres and HA chains undergo continuous decrosslinking – recrosslinking cycles during shear deformation.[29] This dynamic equilibrium simultaneously enhances structural integrity (manifested as elevated storage modulus) while reducing resistance to flow under injection forces.

In addition, comprehensive characterization of injectable hydrogels for dermal application requires rigorous evaluation of critical physiochemical properties including pH, osmolality, residual BDDE content, and HA concentration. These parameters collectively determine biocompatibility and clinical performance. Optimal dermal filler must maintain pH (7.0–7.4) and osmolality (289 ± 6.6 mOsmol per L) within physiological ranges to prevent tissue irritation while ensuing cellular compatibility.[30,31] Though BDDE-mediate crosslinking enhances HA hydrogels durability through covalent network formation, regulatory guidelines mandate either complete elimination of residual BDDE content below the established toxicity threshold of 2 ppm due to its documented mutagenic risks. HA concentration critically influences both rheological properties and bio-integration capacity, with higher concentrations typically correlating with prolonged residence time but requiring balanced injectability.

Comparative analysis of key physicochemical parameters (Table 2) revealed appropriate pH and osmolality in both ISE and PMD systems. Notably, residual BDDE content remained undetectable (<1 ppm), significantly below regulatory limits.

Table 2 The pH, osmolality, HA concentration, and BDDE residue of CHPs fabricated by *in situ* encapsulation (ISE) and post-mixing dispersion (PMD) approaches

| | pH | Osmolality (mOsmol per L) | HA content (mg mL$^{-1}$) | BDDE residual (ppm) |
|---|---|---|---|---|
| ISE | 7.19 | 289 | 18.40 | 0.71 |
| PMD | 7.22 | 296 | 18.34 | 0.89 |

Furthermore, comparable HA concentration (18.40 mg mL$^{-1}$ *vs.* 18.34 mg mL$^{-1}$) between these two approaches, suggesting consistent network density despite differing fabrication methodologies. These findings collectively validate the *in situ* encapsulation approach, as evidenced by Table 2, which documented optimal physiochemical profiles including undetectable BDDE residues, physiological-compliant electrolyte balance, and controlled HA concentration. The synergistic optimization of these characteristics not only fulfills essential criteria for injectable dermal fillers but also underscores the methodology's capability to preserve structural integrity while mitigating biological risks through precision engineering.

## Conclusions

This study successfully engineered crosslinked HA-PLLA composite hydrogels (CHPs) *via* a novel *in situ* encapsulation approach, overcoming critical limitations of conventional post-mixing dispersion (PMD) method. Through an $L_{16}$ ($4^3$) orthogonal experimental design, optimal parameters (3% PLLA, 1.0% BDDE, 48 h crosslinking) were identified, achieving a clinically relevant storage modulus ($G' = 790$ Pa) within 16 experimental iterations – a 75% reduction compared to full-factorial approaches. The *in situ* methodology facilitated interfacial hydrogen bonding between HA hydroxyl/carboxyl groups and PLLA carbonyl moieties, enhancing mechanical resilience (2.3 times higher $G'$ than PMD systems) while maintaining injectability through 27-gauge needles. These hydrogels exhibited prolonged enzymatic resistance, with degradation rates lower than controls, attributed to dense network topology restricting hyaluronidase diffusion. Furthermore, all formulations met stringent biocompatibility criteria, including physiological pH (7.19–7.22), osmolality (289–296 mOsmol per L), and undetectable BDDE residues (<1 ppm), aligning with regulatory standards for dermal fillers. The *in situ* encapsulation approach not only addresses HA hydrogel limitations but also establishes a scalable platform for multifactorial optimization of composite biomaterials. Future studies will focus on *in vivo* functionality

assessment and integration of bioactive motifs to further enhance tissue regeneration and therapeutic outcomes.

## Author contributions

Conceptualization, Jiahong Guo; data curation, Hang Li, Jiahong Guo; investigation, Hang Li, Jiahong Guo; writing – original draft preparation, Jiahong Guo; writing – review & editing, Jiahong Guo; resources, Feifei Wang; supervision, Feifei Wang.

## Conflicts of interest

There are no conflicts to declare.

## Data availability

All relevant data supporting this article have been included in the manuscript and data will be made available on request.

Supplementary information: The morphologies of pure PLLA microspheres and CHPs with different PLLA feed loading with higher magnification, are included here. See DOI: **https://doi.org/10.1039/d5ra04259c**.

## Acknowledgements

The authors gratefully acknowledge funding from the Independent Research Fund of Yunnan Characteristic Plant Extraction Laboratory (2023YKZY005 and 2024YKZY001).

## References

1 N. N. Yuan, K. Shao, S. Huang and C. Chen, *Int. J. Biol. Macromol.*, 2023, **240**, 124321.
2 S. Q. Yu, S. Wang, L. X. Xia, H. W. Hu, M. Y. Zou, Z. W. Jiang, J. H. Chi, Y. J. Zhang, H. J. Li, C. Z. Yang, W. S. Liu and B. Q. Han, *Int. J. Biol. Macromol.*, 2022, **208**, 159.
3 G. Qin, R. N. Wu, Q. Q. Wang, M. Z. Sun, Y. Li, S. Duan and F. J. Xu, *ACS Biomater. Sci. Eng.*, 2024, **10**, 7657.
4 J. Faivre, A. I. Pigweh, J. Iehl, P. Maffert, P. Goekjian and F. Bourdon, *Expert Rev. Med. Devices*, 2021, **18**, 1175.
5 M. Murugesan, R. Mathiyalagan, Z. M. Ramadhania, J. Nahar, C. H. Luu, V. H. G. Phan, D. C. Yang, Q. H. Zhou, S. Chan Kang and T. Thambi, *Bioact. Mater.*, 2025, **49**, 154.
6 S. Gou, A. Porcello, E. Allémann, D. Salomon, P. Micheels, O. Jordan and Y. N. Kalia, *Pharmaceutics*, 2023, **15**, 1708.
7 P. Žádníková, R. Šínová, V. Pavlík, M. Šimek, B. Šafránková, M. Hermannová, K. Nešporová and V. Velebný, *Biomolecules*, 2022, **12**, 251.
8 J. J. Zhao, Z. W. Chen, X. S. Li, Z. R. Tong, Z. J. Xu, P. S. Feng and P. Wang, *J. Biomed. Mater. Res., Part A*, 2024, **112**, 721.
9 J. Z. Huang, J. M. Xue, J. M. Huang, X. X. Zhang, H. J. Zhang, L. Du, D. Zhai, Z. G. Huan, Y. F. Zhu and C. T. Wu, *Bioact. Mater.*, 2025, **44**, 256.
10 F. Ghorbani, A. Zamanian, A. Behnamghader and M. Daliri Joupari, *Mater. Sci. Eng., C*, 2020, **112**, 110906.
11 H. Y. Jang, J. Y. Shin, S. H. Oh, J. H. Byun and J. H. Lee, *ACS Biomater. Sci. Eng.*, 2020, **6**, 5172.
12 B. Nowag, G. Casabona, S. Kippenberger, N. Zöller and T. Hengl, *J. Cosmet. Dermatol.*, 2023, **22**, 426.
13 Y. X. Dong, Y. L. Zhang, H. Yu, L. C. Zhou, Y. A. Zhang, H. B. Wang, Z. C. Hu and S. K. Luo, *Front. Immunol.*, 2024, **15**, 1394530.
14 J. H. Guo, W. Fang and F. F. Wang, *RSC Adv.*, 2023, **13**, 23841.
15 P. Cannata-Ortiz, C. Gracia, Y. Aouad, A. Barat, M. A. Martinez-Gonzalez, G. Rossello, C. Martin-Cleary, B. Fernández-Fernández, L. Requena and A. Ortiz, *Diagn. Pathol.*, 2016, **11**, 2.
16 C. Y. Zhu, Y. T. Zhang, T. Wu, Z. H. He, T. Guo and N. P. Feng, *Acta Pharm.*, 2022, **72**, 135.
17 K. X. Qiu, S. Chen, C. Wang, B. W. Yang and J. H. Jiang, *Polymers*, 2023, **15**, 2898.
18 Y. Q. Wang and Z. W. Ding, *Sci. Rep.*, 2022, **12**, 12121.
19 H. Quan, Y. Guo, R. N. Li, Q. M. Su and Y. Chai, *Sci. Prog.*, 2020, **103**(1), DOI: **10.1177/0036850419881**.
20 K. Y. Gu, K. Y. Yang, C. L. Zhao, Q. Shu and R. Lin, *Heliyon*, 2025, **11**, e42502.
21 K. Jariyavidyanont, Q. Yu, A. Petzold, T. Thurn-Albrecht, R. Glüge, H. Altenbach and R. Androsch, *J. Mech. Behav. Biomed. Mater.*, 2023, **137**, 105546.
22 Z. P. Liu, J. Wang, H. N. Chen, G. Y. Zhang, Z. M. Lv, Y. J. Li, S. J. Zhao and W. L. Li, *Polymers*, 2021, **13**, 3595.
23 E. Capuana, F. Lopresti, M. Ceraulo and V. La Carrubba, *Polymers*, 2022, **14**, 1153.
24 J. H. Guo, W. Fang and F. F. Wang, *Eur. Polym. J.*, 2024, **219**, 113395.
25 A. M. Vasi, M. I. Popa, M. Butnaru, G. Dodi and L. Verestiuc, *Mater. Sci. Eng., C*, 2014, **38**, 177–185.
26 W. Fang, J. H. Guo and F. F. Wang, *New J. Chem.*, 2024, **48**, 18111.
27 Y. Feng, K. Xiao, J. L. Chen, J. J. Lin, Y. Y. He, X. L. He, F. Y. Cheng, Z. Li, J. H. Li, F. Luo, H. Tan and Q. Fu, *Carbohydr. Polym.*, 2023, **320**, 121238.
28 Y. Lee, S. M. Oh, W. Lee and E. J. Yang, *J. Cosmet. Dermatol.*, 2021, **20**, 1551.
29 A. D. Crowell, T. M. FitzSimons, E. V. Anslyn, K. M. Schultz and A. M. Rosales, *Macromolecules*, 2023, **56**, 7795.
30 G. H. Lu, X. S. Miao and L. Dou, *Expert Opin. Drug Metab. Toxicol.*, 2021, **17**, 1103.
31 M. H. Bhuiyan, A. N. Clarkson and M. A. Ali, *Colloids Surf., B*, 2023, **224**, 113193.